Geochemical Journal, Vol. 41, pp. 463 to 474, 2007

Iron speciation and mineral characterization of contaminated sediments by coal mining drainage in Neath Canal, South Wales, United Kingdom

GUODONG ZHENG,[1,2,3]* AKIHITO KUNO,[4] TALIB A. MAHDI,[2] DAVID J. EVANS,[5] MASAAKI MIYAHARA,[3,6] YOSHIO TAKAHASHI,[3] MOTOYUKI MATSUO[4] and HIROSHI SHIMIZU[3]

[1]Key Laboratory of Gas Geochemistry, Institute of Geology and Geophysics, Chinese Academy of Sciences, 382 West Donggang Road, Lanzhou 730000, P.R. China
[2]GRC, School of Engineering, Cardiff University, Cardiff CF24 3AA, U.K.
[3]Department of Earth and Planetary Systems Science, Hiroshima University, Higashi-Hiroshima 739-8526, Japan
[4]Graduate School of Arts and Sciences, The University of Tokyo, 3-8-1 Komaba, Meguro-ku, Tokyo 153-8902, Japan
[5]Department of Biological Chemistry, John Innes Centre, Norwich Research Park, Norwich, NR4 7UH, U.K.
[6]Institute of Mineralogy, Petrology and Economic Geology, Graduate School of Science, Tohoku University, Sendai 980-8578, Japan

(*Received May 17, 2007; Accepted September 12, 2007*)

In the early 1990's, the Neath Canal in South Wales, UK, received large amounts of drainage waters from nearby coal mines, which contributed to its contamination by heavy metals and arsenic. One sediment core and surface sediments were collected from the upstream section of the Neath Canal and characterized for their mineral composition and iron speciation using powder X-ray diffraction (XRD) and Mössbauer spectroscopy. The sediments show three distinctive layers that are defined by their physical properties including color, sediment components and dryness. The upper layer of the sediment (0–22 cm) is a reddish-brown wet precipitate dominated by iron oxides and hydroxides and a high content of arsenic. The middle layer (22–27 cm) is a soft wet deposit of yellow color which mainly contains calcite with sheet silicates (kaolinite) and goethite. Magnesium, calcium and manganese are enriched in this layer whereas iron is depleted compared to the upper layer. The lower part of the core (below 27 cm) is colored gray to dark gray and contains quartz, pyrite and clay minerals, similar to normal aquatic sediments. In addition, this layer also contains abundant coal particles. Silicon, aluminium, titanium, potassium, phosphorus and sodium concentrations are higher whereas iron, manganese, calcium and magnesium are lower in the lower portion of the core compared to the middle and upper layers. Mineral composition, major elements, and iron speciation indicate oxic conditions in the upper and middle layers whereas reducing conditions prevail in the lower layer, which likely control the distribution of hazardous elements. Given the variation of physico-chemical characteristics of the sediments with depth in the canal, different remediation treatments will likely be necessary for each layer of sediments.

Keywords: iron oxide, carbonation, arsenic, coal mining drainage, Neath canal sediments

INTRODUCTION

The redox chemistry of iron plays a major role in the geochemical cycling of many types of elements (anions and cations) in pristine and contaminated aquatic systems. As many studies have shown, iron minerals and/or iron-bearing compounds in marine and terrestrial sediments influence the cycling of carbon and sulfur (Berner, 1984; Berner and Raiswell, 1984; Davison, 1993; Drodt *et al*., 1998) and largely control the fate of toxic elements, such as arsenic (e.g., Fuller *et al*., 1993; Belzile and Tessier, 1990; Raiswell and Canfield, 1998; van der Zee *et al*., 2003). Several kinds of iron oxides and oxyhydroxides, such as ferrihydrite, goethite and hematite, are considered powerful sorbents of arsenic in acid mine drainage (AMD) or acid rock drainage (ARD) and mine-tailings ponds (Acero *et al*., 2006; Gault *et al*., 2005; Sherman and Randall, 2003). On the other hand, carbonation (carbonate mineral formation) has been shown to immobilize many kinds of heavy metals in contaminated soils, sediments and other residues (Alba *et al*., 2001; Bertos *et al*., 2004a; Bonen and Sarkar, 1995; van Gerven *et al*., 2004; Yu *et al*., 2005). At the present time, accelerated carbonation is a developing technology for treating various hazardous materials and it is widely applied for the remediation of many potential toxic elements, such as arsenic (Jing *et al*., 2003), lead (Yin *et al*., 2006), and chromium (Luz *et al*., 2006; Macias *et al*., 1997). More-

*Corresponding author (e-mail: gdzhuk@hotmail.com)

Table 1. Samples from the Neath Canal in Wales, UK

Sample ID	Depth (cm)	Color description	Color code	Moisture (%)	Pore water		LOI (%)	Classification
					pH	Conductivity ($S \cdot cm^{-1}$)		
Cored samples								
TW3-01	0.0–5.0	bright brown	7.5YR 5/8	75.1	7.07	1.183	15.3	upper layer
TW3-02	5.0–10.0	reddish brown	5YR 4/8	78.2	7.68	1.636	9.03	″
TW3-03	10.0–19.0	bright reddish brown	5YR 5/8	82.1	7.68	1.929	9.95	″
TW3-04	19.0–22.0	bright reddish brown	5YR 5/8	85.2	7.84	0.566	13.0	″
TW3-05	22.0–27.0	light yellow orange	7.5YR 8/4	87.2	7.91	2.01	14.0	middle layer
TW3-06	27.0–30.0	olive brown	2.5Y 4/3	57.1	n.w.	n.w.	16.1	lower layer
TW3-07	30.0–37.0	brown black	2.5Y 3/2	30.8	7.74	1.373	13.3	″
TW5-08	40.0–50.0	gray	7.5Y 4/1	27.8	n.w.	n.w.	14.8	″
TW5-09	50.0–60.0	gray	7.5Y 4/1	24.5	7.82	0.534	14.6	″
TW5-10	70.0–75.0	olive black	7.5Y 3/1	21.2	n.w.	n.w.	16.3	″
Top sediment samples								
Iron-1	0.0–1.0	brown-red						Topmost 5 cm sediment
Iron-2	1.0–2.0	brown-red						
Iron-3	2.0–3.0	brown-red						
Iron-4	3.0–4.0	red						
Iron-5	4.0–5.0	red						

n.w.- there was no pore water available.

over, various kinds of carbonate minerals, such as calcite and dolomite, can be generated and accumulated in aquatic environments, which has an impact on the solidification/stabilization (S/S) of the treated materials. However, such a process is dependent on the pH and physicochemical conditions of the sediments. Thus, much attention should be paid to the characterization of AMD or ARD in order to better understand the fate of hazardous elements.

The upper stream of the Neath Canal was impacted by AMD in the early 1990's and the sediments contain ochreous precipitates (Hallberg and Johnson, 2003). Previous investigations revealed that the levels of arsenic, copper, nickel, and zinc, along with iron, exceeded the EPA (European Protection Agency) guidelines for metal content in soils (Mahdi *et al*., 2003). However, those investigations mainly focused on the reddish sediments in the upstream part of the canal and relatively less attention has been paid to the relationship between iron speciation and the distribution of heavy metal pollutants in the Neath Canal sediments. As a result, it is necessary to characterize the vertical profile of the sediments in the polluted portion of canal in order to determine the proper treatment protocol for the canal sediments (Stephens *et al*., 2001a, b). In this paper, Mössbauer spectroscopy and powder X-ray diffraction (XRD) are used to investigate the characteristics and differences of the various mineral phases present in the sediment profile, especially the iron-rich species present in the canal sediments from the uppermost portion of the Neath Canal. The impacts of those mineral phases on element distribution are also discussed with respect to potential remediation treatments of the contaminated canal sediments.

Study Site and Sampling

Neath Canal, located in the Neath Valley in South Wales, was opened in 1856 as a supply of industrial water. It is an important water supply conduit to various industries in the Neath-Port Talbot area on the Neath River estuary. The Neath Valley and its adjacent area used to be extremely active in coal mining during the industrial period (Fowler *et al*., 1999).

The old Ynysarwed adit close to the village of Ynysarwed, mid-Glamorgan, South Wales has been releasing coal-mining tunnel water since the early 1990's following the closure of several coal mines in the area (Hallberg and Johnson, 2003). As a result, a 7 km stretch of the Neath Canal between Abergarwed and Toonna in the Neath valley has been affected. One major pollution incident also happened in the spring of 1993 when a large minewater discharge occurred. The minewater discharge resulted in a characteristic orange-yellow (rust colored) blanketing deposit enriched in iron and hazardous elements, such as arsenic, copper, nickel, and zinc. The N&T Society and Neath Port Talbot Council have planned to

restore the upper part of the Neath Canal by moving the contaminated sediments to a landfill. However, in order to satisfy the environmental control regulations, the pollutants must be removed from the contaminated dredged sediments prior to their discharge in landfill areas.

Based on the general characteristics and distribution of the contaminated sediments in the canal, the most upstream part of the Neath Canal was selected for this study. Several cores were taken, but core TW3 (located at Treatment Works station) was studied in further detail because it was representative of the sediments present in the contaminated area. The core (Table 1) was collected using a plastic tube with a 2.5 cm inner diameter and the samples were numbered TW3-01 through TW3-07. They represent the upper 37 cm of sediments. Additional sediment samples in the canal were obtained from holes that were dug nearby. The surface sediments were removed with a shovel and fresh samples were collected. These samples are labeled as TW5-08, TW5-09, and TW5-10. In addition, the top portion of the sediments (5 cm) at the sampling point was sampled every 1 cm and labeled Iron-1 through Iron-5. All sampling points were located within an area less than 4 m^2 in the main stream of the canal.

Analyses

A sub-set of samples was freeze-dried after being homogenized and centrifuged under nitrogen atmosphere in order to separate pore water. Dried samples were pulverized into powder using an agate mortar and pestle and then stored under dry conditions in a closed desiccator to avoid further potential contamination and chemical variation of the original iron components. The moisture content and loss on ignition (LOI) were measured on another subset of fresh samples by heating about 5 g of sediments in pottery crucibles using an oven at 105°C for 1 hour and then in a Muffle furnace at 550°C for 18 hours.

For ^{57}Fe Mössbauer measurement, 100–110 mg of the freeze-dried powdered samples (without any chemical pretreatment) was gently pressed into a brass sample holder (16 mm in diameter, 1 mm thick). The Mössbauer spectra were obtained with an Austin Science S-600 Mössbauer spectrometer using a γ-ray source of 1.11 GBq ^{57}Co/Rh at a consistent temperature (293 K) or liquid helium temperature (4.2 K). Spectra were fitted to Lorentzian line shapes using standard line shape fitting routines. Half-width and peak intensity of each quadruple doublet was constrained to be equal. Isomer shifts were expressed with respect to the centroid of the spectrum of metallic iron foil at 298 K.

X-ray powder diffraction (XRD) was used to determine the mineral composition of the sediments using a MAC M18XHF diffractometer with Cu-Kα radiation (40 kV, 100 mA). A portion of the freeze-dried samples was crushed to fine powder using a small clean mortar and then mounted on an aluminum holder for XRD analysis. Powder XRD scans were performed with the fine powder samples and run from 2 to 80° 2θ at a step scan of 0.020° 2θ and 1.00 s counting time per step. A portion of the fine powdered samples was also heated at 500°C for an hour and then scanned by XRD in order to identify kaolinite and smectite (More and Reynolds, 1997). The concentration of major elements was measured with the alkaline fused bead method using X-ray fluorescence (XRF). The fused glass bead for XRF measurement was prepared from the powdered freeze-dried bulk sample (2.000 g) mixed with Flux No. 100B SPECTROFLUX (4.000 g containing 80% $Li_2B_4O_7$ and 20% $LiBO_2$) and $LiNO_3$ (0.60 g), which was melted in a platinum crucible at 1200–1210°C using a TK-4100 Bead & Fuse-Sampler. The concentrations of selected heavy metals were determined using inductively coupled plasma-mass spectroscopy (ICP-MS) after acidic digestion of the samples. Chemical procedures for the sample digestion are described in Zheng *et al*. (2001).

Results and Discussion

Sediment physical characteristics

A series of cores revealed the presence of three distinctive layers of sediments in the canal. The thickness of the upper and middle layers decreases away from the minewater discharge point, where the representative core TW3 was taken (Table 1). The upper layer of the sediments (i.e., 0–22 cm) consists of a soft muddy precipitate of brown-reddish color, which looks like an ochreous sludge. The moisture content is high, and increases with depth. However, the surface sediments of the topmost layer (a few cm) has a darker color likely due to the newly deposited organic matter, such as vegetation remains, mixed with sediment particles from the slope and some coal particles carried by the AMD from the damaged mine tunnels. The middle layer (i.e., 22–27 cm) is also soft but has a bright yellowish color when it is wet and the deposit is clearly different from both the upper and lower layers and contains the highest moisture content, 87.2% (Table 1) of the whole sedimentary column. The deposit is easily broken when it is wet, but becomes hard and very sticky during powdering after being dried. The two upper layers clearly represent sediments that formed after the mine discharge in 1993. In contrast, the lower layer of sediment varies from gray to deep gray, and then to black with depth and likely represents the old canal sediments prior to the discharge in 1993. The moisture contents of the lower layer are lower than the upper two layers and decrease with depth (Table 1 and Fig. 1). The sharp variation of moisture content between the two upper layers and the old canal sediments may indicate

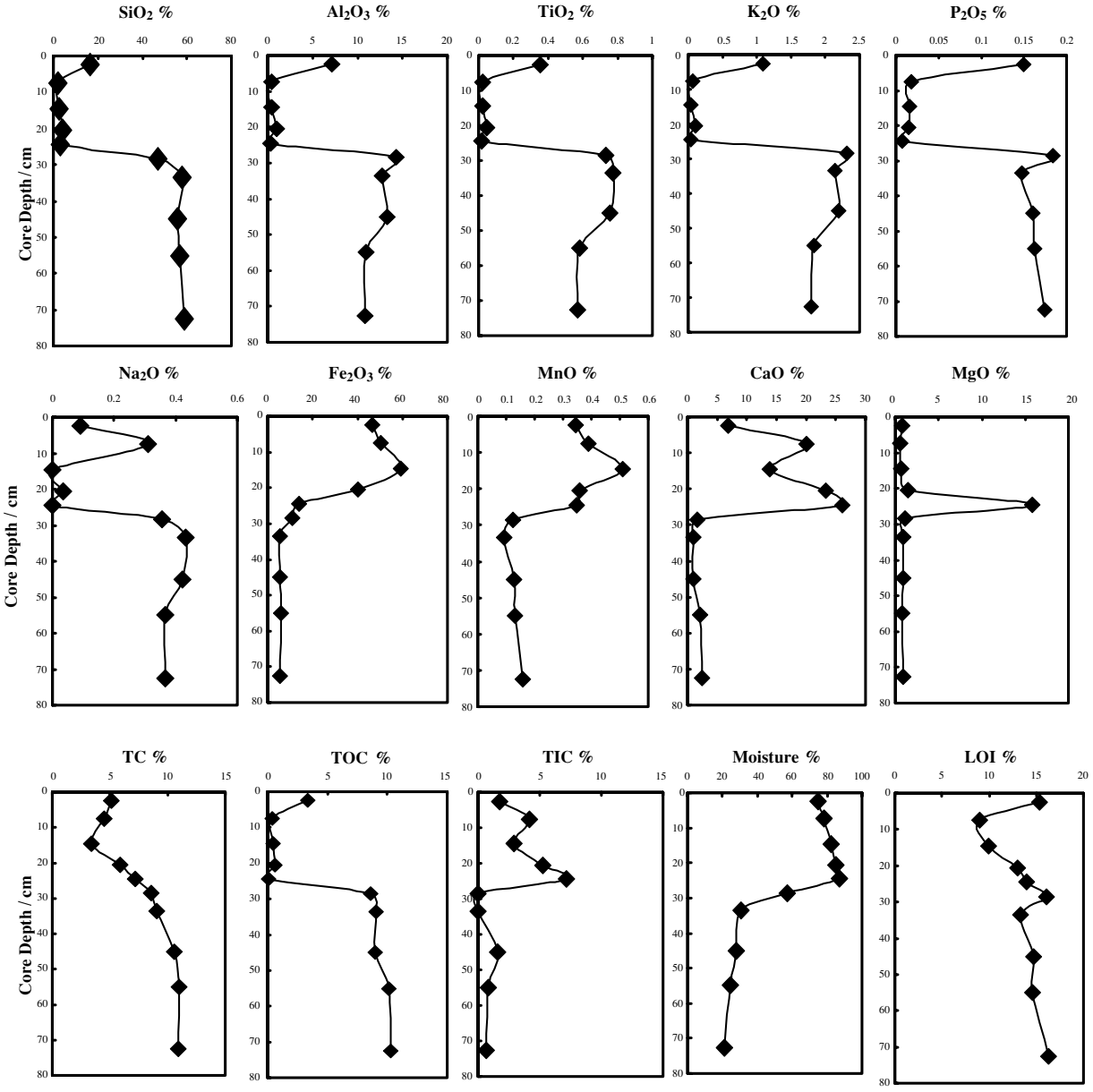

Fig. 1. Vertical profiles of major elements, moisture, loss on ignition (LOI), total organic carbon (TOC), total inorganic carbon (TIC) and total carbon (TC) of the Neath canal sediments.

that the vertical circulation and exchange of pore water is very weak between the layers even though water constantly flows in the canal. The presence of clay minerals in the sediments (see Subsection "Mineral composition of the sediments") appears to reduce the porosity of the sediments. In addition, there are abundant artificial particles, such as concrete, broken glass bottles, and shining coal particles in the lower layer of sediments (below 27 cm) deposited during the early stage of coal mining and sailing operations since the canal was also used for coal transportation.

Mineral composition of the sediments

The XRD patterns of the sediments from core TW3 are shown in Fig. 2. Quartz, calcite, and goethite dominate the sediments, along with some other minor minerals. It is clear that the three layers of sediments have distinctive XRD patterns based on the composition and width of the reflection peaks. The samples from the upper layer (TW3-01 through TW3-04) are dominated by calcite and goethite (Fig. 2A). Only the surface sample TW3-01 contains quartz and some clay minerals. The sample of the middle layer, TW3-05 displays stronger peaks for calcite

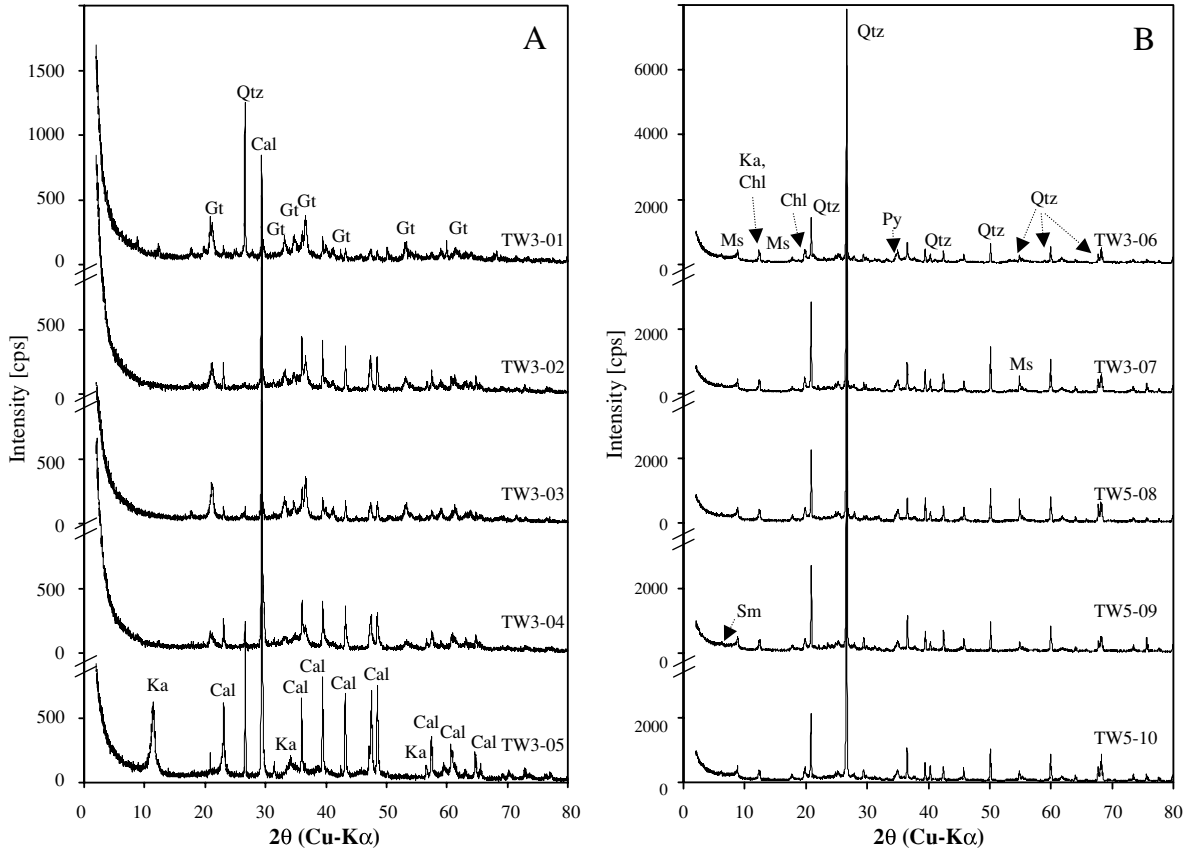

Fig. 2. XRD patterns of the sediments from the Neath Canal. A, samples of the upper and middle sections of core; B, samples of the lower portion of the same core. Ka, kaolinite; Qtz, quartz; Ms, muscovite; Cal, calcite; Gt, goethite; Py, pyrite; Sm, smectite; Chl, chlorite.

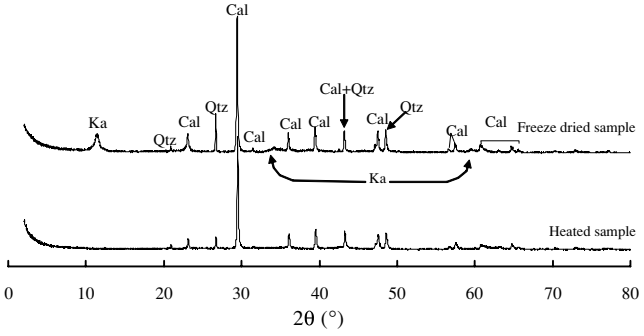

Fig. 3. XRD patterns of the freeze-dried and heated sediments from the middle layer of the Neath canal sediment. Ka, kaolinite; Qtz, quartz; Cal, calcite.

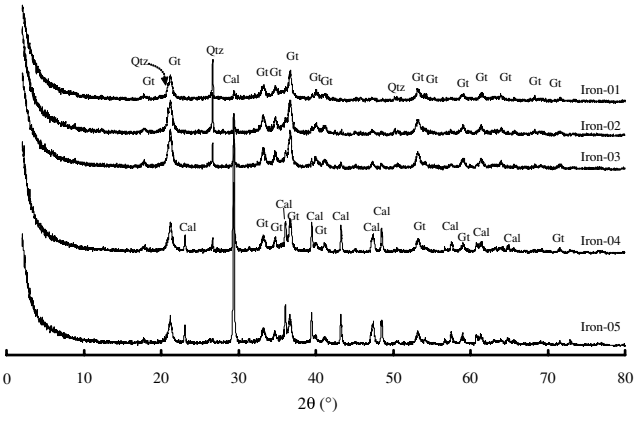

Fig. 4. XRD patterns obtained for the surface samples Iron-01 to Iron-05. Qtz, quartz; Cal, calcite; Gt, goethite.

than those present in the upper layer samples. In addition, there are also distinct reflection peaks corresponding to kaolinite, especially the wide peak between 10.5–12° (Figs. 2A and 3). In order to confirm this mineral phase, the yellow deposit was heated at 500°C for 1 hour (Fig. 3), which led to the disappearance of those peaks and confirmed the presence of the sheet silicate mineral kaolinite (More and Reynolds, 1997). All reflection peaks for the samples from the upper and middle layers are rela-

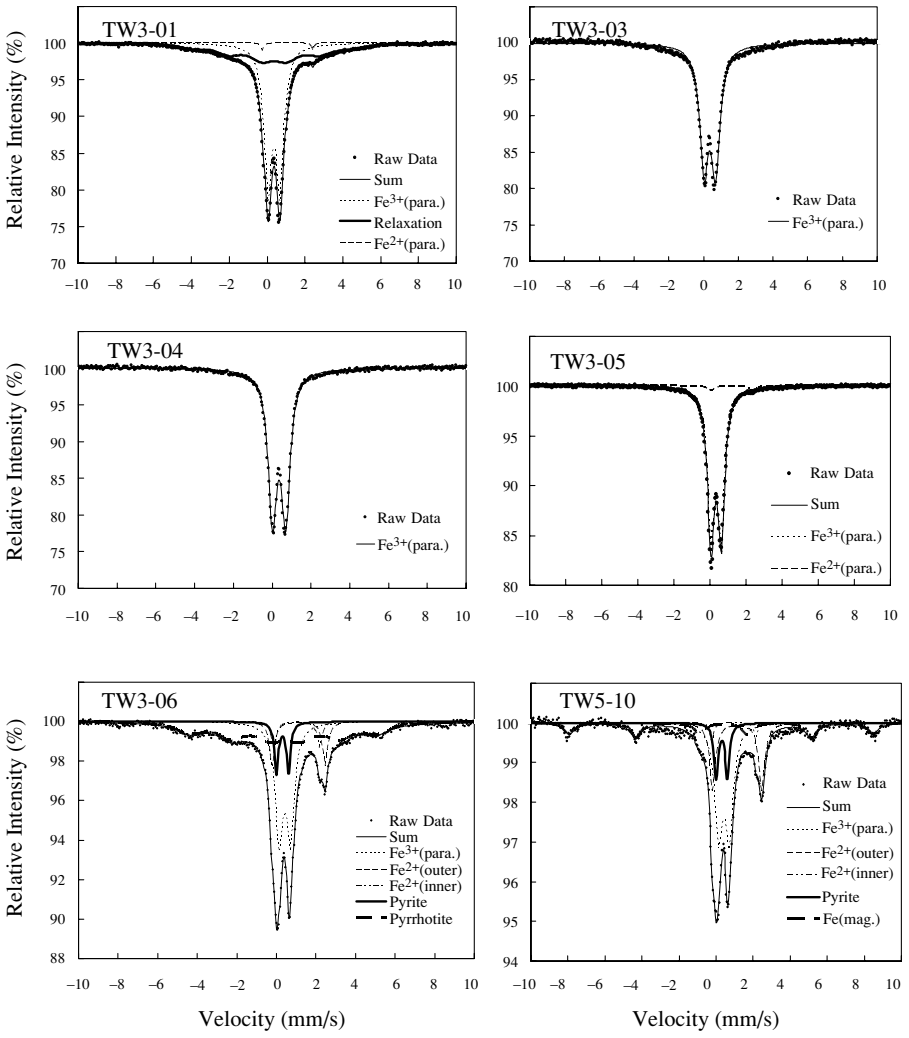

Fig. 5. Mössbauer spectra for selected samples collected from the Neath Canal, South Wales. Vertical axis, transmission (%); horizontal axis, isomer shift mm/s.

tively weaker compared with those of the lower layer. However, the reflection peaks for calcite, goethite, and also kaolinite are sharp, indicating that these minerals are crystalline and formed as a result of diagenetic reactions in less than 10 years after the mine water discharge accident.

Quartz, pyrite, chlorite, kaolinite, muscovite, and smectite were identified in the samples from the lowest layer (TW3-06, 07 and TW5-08, 09 and 10) (Fig. 2B). These minerals are common components of aquatic clastic sediments. The existence of pyrite and chlorite indicate the presence of reducing conditions in the sediments (Berner 1984; Berner and Raiswell 1984). The XRD pattern of each sample from the lower layer is very similar, showing a similar composition of major minerals in the old canal sediments. The results confirmed the physical observations (Subsection "Sediment physical characteristics"), i.e., the two upper layers clearly differ in their mineralogical contents from the bottom layer.

Figure 4 shows the XRD patterns of the surface sediment samples (Iron-1 to Iron-5; Table 1) in the canal, which were collected from the topmost 5 cm of sediments. Newly formed minerals, such as calcite and goethite, clearly dominate. The first three samples (Iron-1 to Iron-3) are predominantly composed of goethite with very little quartz and calcite, whereas the other two samples (Iron-4 and Iron-5) mainly contain calcite and goethite, displaying peaks of various intensity.

Iron speciation

Selected Mössbauer spectra of samples measured at room temperature (Fig. 5) show several kinds of iron species, including four overlapping doublets, two sextets and one relaxation spectrum. The curve fitting of these seven

Table 2. Mössbauer parameters of the iron components in the cored sediment samples collected from the Neath Canal, South Wales (measured at 293 K)

Sample ID	Total peak area/% mm s^{-1}	Iron species	Relative content %	IS/mm s^{-1}	QS/mm s^{-1}	HW/mm s^{-1}	Hi/T
TW3-01	23.92 ± 0.17	*para*-Fe^{3+}	62.05 ± 0.93	0.365 ± 0.001	0.649 ± 0.002	0.500 ± 0.004	
		relaxation	36.74 ± 0.95	0.283 ± 0.035	–0.171 ± 0.058	1.586 ± 0.074	25.71 ± 0.35
		para-Fe^{2+}	1.21 ± 0.09	1.084 ± 0.011	2.655 ± 0.023	0.188 ± 0.035	
TW3-02	22.56 ± 0.09	*para*-Fe^{3+}	100.00 ± 0.00	0.359 ± 0.001	0.676 ± 0.002	0.557 ± 0.004	
TW3-03	19.88 ± 0.12	*para*-Fe^{3+}	100.00 ± 0.00	0.365 ± 0.002	0.668 ± 0.004	0.609 ± 0.007	
TW3-04	21.21 ± 0.07	*para*-Fe^{3+}	100.00 ± 0.00	0.359 ± 0.001	0.679 ± 0.002	0.537 ± 0.003	
TW3-05	13.86 ± 0.06	*para*-Fe^{3+}	96.83 ± 0.17	0.347 ± 0.001	0.577 ± 0.002	0.455 ± 0.003	
		para-Fe^{2+}	3.17 ± 0.17	1.207 ± 0.010	2.301 ± 0.020	0.474 ± 0.029	
TW3-06	15.60 ± 0.30	*para*-Fe^{3+}	35.73 ± 0.63	0.422 ± 0.009	0.587 ± 0.004	0.489 ± 0.009	
		para-Fe^{2+}(outer)	9.80 ± 0.25	1.120 ± 0.006	2.682 ± 0.014	0.343 ± 0.020	
		para-Fe^{2+}(inner)	5.39 ± 0.23	1.021 ± 0.010	2.312 ± 0.022	0.321 ± 0.037	
		pyr-Fe^{2+}	8.19 ± 0.48	0.307 ± 0.000	0.610 ± 0.000	0.247 ± 0.028	
		pyrrhotite	40.89 ± 0.69	0.393 ± 0.024	–0.111 ± 0.035	1.618 ± 0.059	29.01 ± 0.21
TW3-07	9.56 ± 0.43	*para*-Fe^{3+}	32.45 ± 1.24	0.419 ± 0.014	0.579 ± 0.006	0.503 ± 0.013	
		mag-Fe^{3+}	37.03 ± 1.86	0.341 ± 0.084	–0.077 ± 0.132	2.558 ± 0.234	50.49 ± 0.75
		para-Fe^{2+}(outer)	19.16 ± 0.66	1.146 ± 0.006	2.606 ± 0.008	0.391 ± 0.019	
		para-Fe^{2+}(inner)	3.57 ± 0.24	0.943 ± 0.010	2.418 ± 0.021	0.235 ± 0.039	
		pyr-Fe^{2+}	7.80 ± 0.82	0.307 ± 0.000	0.610 ± 0.000	0.283 ± 0.051	
TW5-08	13.93 ± 0.21	*para*-Fe^{3+}	44.45 ± 0.54	0.460 ± 0.007	0.521 ± 0.005	0.594 ± 0.010	
		mag-Fe^{3+}	7.23 ± 0.35	0.358 ± 0.015	–0.208 ± 0.030	0.453 ± 0.047	51.18 ± 0.12
		para-Fe^{2+}(outer)	19.57 ± 0.36	1.126 ± 0.003	2.688 ± 0.010	0.351 ± 0.014	
		para-Fe^{2+}(inner)	21.08 ± 0.41	1.071 ± 0.005	2.218 ± 0.018	0.448 ± 0.022	
		pyr-Fe^{2+}	7.68 ± 0.41	0.307 ± 0.000	0.610 ± 0.000	0.257 ± 0.034	
TW5-09	9.31 ± 0.27	*para*-Fe^{3+}	30.94 ± 0.88	0.427 ± 0.014	0.576 ± 0.007	0.508 ± 0.013	
		mag-Fe^{3+}	41.43 ± 1.08	0.291 ± 0.035	–0.073 ± 0.063	1.790 ± 0.134	50.33 ± 0.30
		para-Fe^{2+}(outer)	17.15 ± 0.46	1.152 ± 0.009	2.621 ± 0.015	0.433 ± 0.026	
		para-Fe^{2+}(inner)	4.16 ± 0.27	0.957 ± 0.013	2.365 ± 0.028	0.254 ± 0.045	
		pyr-Fe^{2+}	6.32 ± 0.65	0.307 ± 0.000	0.610 ± 0.000	0.248 ± 0.053	
TW5-10	6.55 ± 0.27	*para*-Fe^{3+}	40.73 ± 1.02	0.428 ± 0.016	0.591 ± 0.006	0.523 ± 0.012	
		mag-Fe^{3+}	19.24 ± 0.74	0.340 ± 0.017	–0.142 ± 0.034	0.648 ± 0.059	50.81 ± 0.14
		para-Fe^{2+}(outer)	21.92 ± 0.53	1.136 ± 0.008	2.653 ± 0.015	0.419 ± 0.020	
		para-Fe^{2+}(inner)	3.74 ± 0.29	0.959 ± 0.017	2.355 ± 0.035	0.234 ± 0.052	
		pyr-Fe^{2+}	11.37 ± 0.96	0.307 ± 0.000	0.610 ± 0.000	0.268 ± 0.044	

components is reliable because the Chi-squared values are sufficiently small (747.7–3389). The doublets with a smaller quadrupole splitting are ascribed to either paramagnetic high-spin ferric iron (*para*-Fe^{3+}) or to iron in pyrite (*pyr*-Fe^{2+}). The former one, *para*-Fe^{3+}, probably corresponds to iron in clay minerals and/or hydrated Fe(III) oxides (Maning and Ash, 1979). Based on the Mössbauer results and XRD patterns (Fig. 2), the *para*-Fe^{3+} of the samples TW3-01 through TW3-04 likely originates from iron present in goethite whereas the *para*-Fe^{3+} of the other samples are mainly from ferric iron in clay minerals (Table 2). The ferrous iron in pyrite was fitted using the following constrained Mössbauer parameters at 293 K; isomer shift (IS) 0.307 mm/s and quadrupole splitting (QS) 0.610 mm/s. Pyrite was considered absent when the calculated peak area of *pyr*-Fe^{2+} was lower than the detection limit, calculated as three times larger than the standard deviation of the baseline count (Kuno *et al.*,

1998). The doublets with a larger quadrupole splitting were attributable to paramagnetic high-spin ferrous iron, *para*-Fe^{2+}(inner) and *para*-Fe^{2+}(outer), respectively. According to their Mössbauer parameters, the *para*-Fe^{2+}(outer) with higher IS, QS, and half-width (HW) may indicate the iron in clay minerals and/or oxide, whereas the *para*-Fe^{2+}(inner) with lower IS, QS and HW may indicate ferrous iron in an organo-iron complex (Matsuo, 1994). For the sextets, at least two kinds of iron minerals can be identified as hematite and pyrrhotite according to their Mössbauer parameters. In addition, one iron species cited as relaxation was also identified (Table 2, Fig. 5). Because of their asymmetry, these spectra could not be properly fitted with distributions of quadrupole splitting having identical isomer shifts, a model that has been proven suitable to fit the room temperature spectra of most poorly crystalline iron oxides (Bigham *et al*., 1990) as a result of relaxation. This species is poorly crystalline and/or amorphous iron oxides, being mostly hydrous ferric oxide (HFO).

In order to further distinguish the various types of iron oxyhydroxides in the samples, cryogenic ^{57}Mössbauer spectroscopy was used for the surface samples collected from the topmost deposit. All the topmost samples were identified with a sextet at liquid helium temperature, which is the paramagnetic ferric iron of hematite in superfine particles (<100 Å), noted as a superparamagnetic effect as described by several researchers (Kündig and Bömmel, 1966; Zheng *et al*., 2001; van Der Zee, 2003). It indicates the formation and deposition of very fine-grained hematite in the AMD sedimentary environment, which cannot be identified by XRD due to its small particle size, as suggested by the superparamagnetic effect.

The vertical distribution of all iron species in the sediment core TW3 is illustrated in Fig. 6. The profile shows that not only various kinds of iron species co-exist within the sediments, but there are also some systematic variations of the iron species. The upper layer of reddish deposits is dominated by ferric iron in goethite, very fine particles of hematite, and/or hydrous ferric oxide, and very little ferrous iron in the topmost part of the sediments. The middle layer contains mostly goethite and very little ferrous iron along with calcite, whereas the lower layer contains much higher contents of ferrous species, such as the iron in magnetite, pyrrhotite, and also pyrite, indicating more reducing conditions in the deep layer of the sediments. The presence of various iron oxides also indicates that some oxides likely aged and transformed overtime, such as the conversion of hydrous ferric oxide into goethite and/or hematite (Schwertmann, 1973; Schwertmann *et al*., 1982).

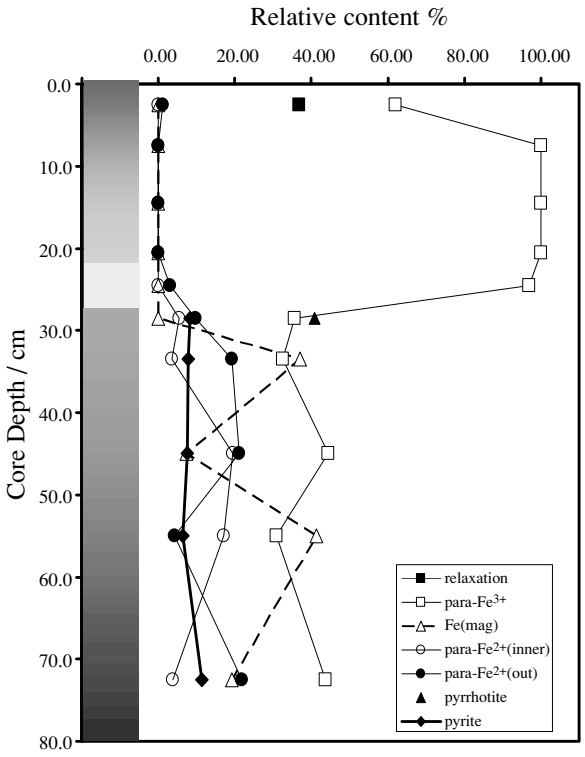

Fig. 6. Vertical distribution of iron species in the Neath canal sediment.

Major element composition

The vertical distribution of major elements in the sediment core is illustrated in Fig. 1. SiO_2, Al_2O_3, TiO_2, K_2O, and P_2O_5 are mainly enriched in the lower layer, and are also elevated in the topmost part of the upper layer; Na_2O also has a similar vertical distribution, with the exception of sample TW3-02. These elements are all lithological elements and their vertical distribution patterns are very similar to those of primary and secondary silicate minerals, such as quartz, kaolinite, chlorite and smectite, representing typical sedimentary particles that have entered the canal prior or during to the pollution event. The decline in organic carbon between 5 and ~27 cm represents a large input of contaminated water which led to the rapid formation of iron oxides during the 1990s by the excess AMD, when the sedimentation rate was likely very high during the period.

On the other hand, Fe_2O_3, MnO, and CaO are enriched in the upper and middle layers whereas MgO is enriched only in the middle layer. According to the XRD data, iron and manganese likely originate from oxides; calcium, and magnesium correspond to newly formed carbonate minerals such as calcite and/or sheet silicates (Haese *et al*., 1997). There is also a positive correlation between CaO plus MgO and total inorganic carbon (TIC) as shown in Fig. 1, which further supports the presence of carbonate minerals in the sediments. The depth distribution of all

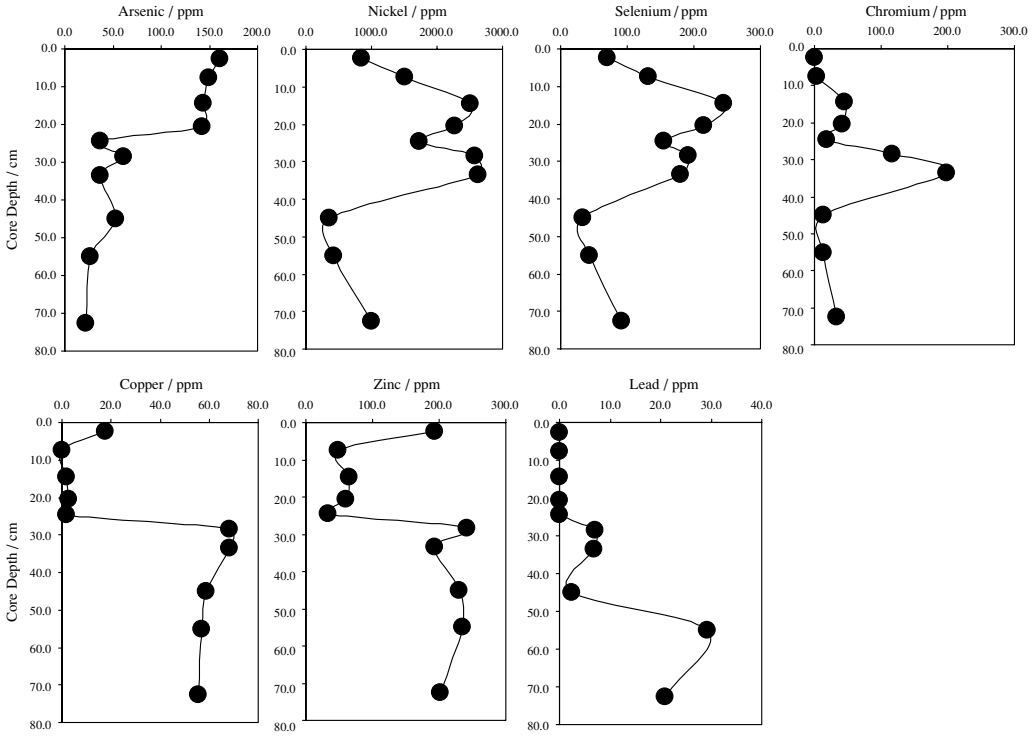

Fig. 7. Vertical profile of heavy metal concentrations in the Neath canal sediment.

major elements clearly indicates the presence of three distinctive layers in the sediments of the canal.

It is clear that the discharge event in 1993 and the ongoing release of AMD entering the canal led to some drastic changes in the chemical and mineralogical characteristics of the sediments. Upon sedimentation and diagenesis, iron, manganese, calcium, and magnesium precipitated over the old canal sediments within the last 10 years. However, the individual distribution of these four elements is different, indicating some difference in their geochemical behavior under such an AMD environment.

Hazardous element distribution

Selected elements, considered as potential pollutants, including As, Cu, Zn, Pb, Cr and Se were analyzed. Figure 7 illustrates the vertical distribution of these elements in the sediments. Arsenic is consistently enriched along with iron in the upper layer of reddish precipitate and its content is almost three times higher than that in the middle and lower layers. Such arsenic enrichment has a positive relationship to ferric iron compounds, especially goethite and fine hematite ($r^2 > 0.79$), which are normally formed and deposited in oxidative environments (Belzile and Tessier, 1990). The arsenic content of the sediments in the lower sediments is relatively constant and may have close relationship to the occurrence of pyrite (Strawn *et al*., 2002). Nickel and selenium show an enrichment in the upper 40 cm of the sediments, which overlaps the lower part of the upper layer, the middle layer, and the upper part of the lower layer. These two elements also show a slow increase with depth below 45 cm. Chromium is relatively high in the upper part of the lower layer with rapid redox change, which appears to indicate that chromium is more stable under reducing conditions (Guo *et al*., 1997) because Cr(III) is more insoluble than Cr(VI) and the reduced chromium should be mainly combined to iron sulfide (Lakatos *et al*., 2002). There is however an increase in chromium content in the deeper part of both the upper and lower layers, which may indicate a change in redox conditions. Copper and zinc are considerably enriched in the lower layer, and also slightly enriched in the surface sediments. There is a close positive correlation between these two metals and the major elements and TOC, indicating that they likely originate from metal sulfides found in coal, which are mixed with the sediments (Carignan and Terrier, 1985; Pickhardt, 1989; Rieder *et al*., 2007). Lead is only elevated in the deep part of the lower layer and most likely originated from sulfide minerals formed under more reducing conditions (Lambert *et al*., 2006).

Based on the above mineralogical and geochemical data, it is clear that the distribution of heavy metals and major elements is closely related to the mineral composi-

tion of the sediments and the iron speciation. The relationship between Fe, Mn, Ca, Mg, and As in the Neath Canal sediments show the preference of trace elements for either iron oxides or calcite as their host phases. The results clearly indicate that lesser amounts of arsenic are incorporated into carbonate minerals under an AMD environment, compared to iron oxides. This is important when considering carbonation as a potential remediation strategy. Carbonation is a natural phenomenon affecting the solidification/stability (S/S) of cementitious materials and has been shown to help immobilize many kinds of heavy metals in contaminated soils, sediments and other kinds of residues. At the present time, accelerated carbonation is a developing technology for treating various hazardous materials and has been widely applied for many potential toxic elements (Enick *et al*., 2001; Meng *et al*., 2001; Jing *et al*., 2003; Bertos *et al*., 2004b; Benedetto *et al*., 2007), including arsenic immobilization with Portland cement or quick lime treatment (Moon *et al*., 2004). Based on the present study, however, it is necessary to consider the long-term stability of S/S treated materials in the environment. As revealed by the vertical distributions of arsenic, iron and calcium (and possibly magnesium) in the Neath Canal sediments, the redox conditions appear to be very similar between the upper reddish layer and the middle yellowish layer, based on the very similar ratios of Fe(III)/Fe(II). However, the total arsenic content is sharply different between these two same layers, i.e., 143–161 ppm in the upper layer and only 36.4 ppm in the middle layer. The upper layer, dominated by iron oxides, contains more arsenic than the calcite-rich middle layer. This may be due to the release of arsenic from carbonate minerals and/or to the preferential sorption of arsenic to iron oxides (Belzile and Tessier, 1990). Thus, carbonation, under the conditions prevailing in the canal, might not permanently trap arsenic, especially if water flowing through the sediments destabilizes the carbonate-rich minerals and mobilizes the arsenic. As a result, much attention should be paid to the site selection for arsenic S/S treated materials.

SUMMARY

The Neath Canal sediments from our study site can be vertically divided into three layers with different sedimentary characteristics. The upper layer, 0–22 cm, is a soft precipitate of brown-reddish color; iron oxides and hydroxides of very fine size dominate, along with arsenic. The middle layer, 22–27 cm, is a soft deposit of yellow color and contains kaolinite, calcite and hematite. The lower layer, below 27 cm, is a gray to dark gray material and contains quartz, pyrite and coal particles. The upper two layers represent precipitated mud from AMD since the discharge event, and contain high concentrations of arsenic, copper and selenium. The lower part is the old canal sediment deposited before the AMD event in 1993, with general reducing characteristics. Our study provides useful information with respect to the remediation of the Neath Canal polluted sediments. Given the existence of various physico-chemical and mineralogical characteristics, each layer of the sediments will require different treatment.

Acknowledgments—We would like to thank Prof. Danielle Fortin, the editor of our manuscript, Dr. Fenghua Zhao and two anonymous reviewers for their comments and constructive suggestions. Prof. Hywel R. Thomas and Prof. Raymond N. Yong supervised the project. Miss Kou Weiwei and Mr. Rao Martand Singh provided assistance in the field. GRP, based at Cardiff University, supported the field investigation and the Japan Society for the Promotion of Science (JSPS) supplied a Fellowship to G.Z. for research in Hiroshima University in 2003–2005. G.Z. also acknowledges the financial support from the Chinese Academy of Sciences, "100-Tallent" program to perform research work in 2006–2009. The Biotechnology and Biological Sciences Research Council, UK, are thanked for their support (D.J.E.).

REFERENCES

Acero, P., Ayora, C., Torrentó, C. and Nieto, J.-M. (2006) The behavior of trace elements during schwertmannite precipitation and subsequent transformation into goethite and jarosite. *Geochim. Cosmochim. Acta* **70**, 4130–4139.

Alba, N., Vázquez, E., Gassó, S. and Baldasano, J. M. (2001) Stabilization/solidification of MSW incineration residues from facilities with different air pollution control systems. Durability of matrices versus carbonation. *Waste Management* **21**, 313–323.

Belzile, N. and Tessier, A. (1990) Interactions between arsenic and iron oxyhydroxides in lacustrine sediments. *Geochim. Cosmochim. Acta* **54**, 103–109.

Benedetto, F. D., Costagliola, P., Benvenuti, M., Lattanzi, P., Romanelli, M. and Tanelli, G. (2007) Arsenic incorporation in natural calcite lattice: Evidence from electron spin echo spectroscopy. *Earth Planet. Sci. Lett.* **246**, 458–465.

Berner, R. A. (1984) Sedimentary pyrite formation: an update. *Geochim. Cosmochim. Acta* **48**, 605–615.

Berner, R. A. and Raiswell, R. (1984) C/S methods for distinguishing freshwater rocks from marine sedimentary rocks. *Geology* **12**, 365–368.

Bertos, M. F., Li, X., Simons, S. J. R., Hills, C. D. and Carey, P. J. (2004a) Investigation of accelerated carbonation for the stabilisation of MSW incinerator ashes and the sequestration of CO_2. *Green Chem.* **6**, 428–436.

Bertos, M. F., Simons, S. J. R., Hills, C. D. and Carey, P. J. (2004b) A review of accelerated carbonation technology in the treatment of cement-based materials and sequestration of CO_2. *Journal of Hazardous Materials* **B112**, 193–205.

Bigham, J. M., Schwertmann, U., Carlson, L. and Murad, E. (1990) A poorly crystallized oxyhydroxysulfate of iron formed by bacterial oxidation of Fe(II) in acid mine wa-

ters. *Geochim. Cosmochim. Acta* **54**, 2743–2758.
Bonen, D. and Sarkar, S. L. (1995) The effects of simulated environmental attack on immobilization of heavy metals doped in cement-based materials. *Journal of Hazardous Materials* **40**, 321–335.
Carignan, R. and Terrier, A. (1985) Zinc deposition in acid lakes: the role of diffusion. *Science* **228**, 1524–1526.
Davison, W. (1993) Iron and manganese in lakes. *Earth-Science Reviews* **34**,119–163.
Drodt, M., Lougear, A., Trautwein, A. X., König, I., Suess, E. and Bender, K. C. (1998) Studies of iron in deep-sea sediments by Mössbauer spectroscopy. *Hyperfine Interact.* **117**, 383–403.
Enick, R. M., Beekman, E. J., Shi, C. M., Xu, J. H. and Chordia, L. (2001) Remediation of metal-bearing aqueous waste streams via direct carbonation. *Energy Fuels* **15**, 256–262.
Fowler, P. and Gayer, R. A. (1999) The association between tectonic deformation, inorganic composition and coal rank in the bituminous coals from the South Wales coalfield, United Kingdom. *Int. J. Coal Geol.* **42**, 1–31.
Fuller, C. C., Davis, J. A. and Waychunas, G. A. (1993) Surface chemistry of ferrihydrite: part 2. Kinetics of arsenate adsorption and coprecipitation. *Geochim. Cosmochim. Acta* **57**, 2271–2282.
Gault, A. G., Cooke, D. R., Townsend, A. T., Charnock, J. M. and Polya, D. A. (2005) Mechanisms of arsenic attenuation in acid mine drainage from Mount Bischoff, western Tasmania. *Science of The Total Environment* **345**, 219–228.
Guo, T. Z., DeLaune, R. D. and Patrick, W. H. (1997) The influence of sediment redox chemistry on chemically active forms of arsenic, cadmium, chromium, and zinc in estuarine sediment. *Environ. Int.* **23**, 305–316.
Haese, R. R., Wallmann, K., Dahmke, A., Kretzmann, U., Müller, P. J. and Schulz, H. D. (1997) Iron species determination to investigate early diagenetic reactivity in marine sediments. *Geochim. Cosmochim. Acta* **61**, 63–72.
Hallberg, K. B. and Johnson, D. B. (2003) Novel acidophiles isolated from moderately acidic mine drainage waters. *Hydrometallurgy* **71**, 139–148.
Jing, C., Korfiatis, G. P. and Meng, X. (2003) Immobilization mechanisms of arsenate in iron hydroxide sludge stabilized with cement. *Environ. Sci. Technol.* **37**, 5050–5056.
Kündig, W. and Bömmel, H. (1966) Some properties of supported small α-Fe_2O_3 particles determined with the Mössbauer Effect. *Phys. Rev.* **142**, 327–333.
Kuno, A., Matsuo, M. and Takano, B. (1998) Mössbauer spectroscopic study on vertical distribution of iron components in estuarine sediments collected from Tama River in Tokyo. *Hyperfine Interact.* **C3**, 328–331.
Lakatos, J., Brown, S. D. and Snape, C. E. (2002) Coals as sorbents for the removal and reduction of hexavalent chromium from aqueous waste streams. *Fuel* **81**, 691–698.
Lambert, T. W., Guyn, L. and Lan, S. E. (2006) Development of local knowledge of environmental contamination in Sydney, Nova Scotia: Environmental health practice from an environmental justice perspective. *Science of The Total Environment* **368**, 471–484.
Luz, C. A., Rocha, J. C., Cheriaf, M. and Pera, J. (2006) Use of sulfoaluminate cement and bottom ash in the solidification/stabilization of galvanic sludge. *Journal of Hazardous Materials* **136**, 837–845.
Macias, A., Kindness, A. and Glasser, F. P. (1997) Impact of carbon dioxide on the immobilization potential of cemented wastes: Chromium. *Cement and Concrete Research* **27**, 215–225.
Mahdi, T. A., Zheng, G. and Francis, R. W. (2003) Neath Canal Sediments—A report submitted to the WDA, Report Ref GRP/WP6.3/003.
Matsuo, M., Kobayashi, T. and Tsurumi, M. (1994) Mössbauer spectroscopic characterization of iron components in paddy soil. *Hyperfine Interact.* **84**, 533–537.
Meng, X. G., Korfiatis, G. P., Jing, C. Y. and Christodoulatos, C. (2001) Redox transformations of arsenic and iron in water treatment sludge during aging and TCLP extraction. *Environ. Sci. Technol.* **35**, 3476–3481.
Moon, D. H., Dermatas, D. and Menounou, N. (2004) Arsenic immobilization by calcium-arsenic precipitates in lime treated soils. *Science of the Total Environment* **330**, 171–185.
More, D. M. and Reynolds, R. C., Jr. (1997) *X-ray Diffraction and the Identification and Analysis of Clay Minerals*. 227–260, Oxford University Press, Oxford, New York, 371 pp.
Pickhardt, W. (1989) Trace elements in minerals of German bituminous coals. *Int. J. Coal Geol.* **14**, 137–153.
Raiswell, R. and Canfield, D. E. (1998) Sources of iron for pyrite formation in marine sediments. *Am. J. Sci.* **298**, 219–245.
Rieder, M., Crelling, J. C., Šustai, O., Drábek, M., Weiss, Z. and Klementová, M. (2007) Arsenic in iron disulfides in a brown coal from the North Bohemian Basin, Czech Republic. *Int. J. Coal Geol.* **71**, 115–121.
Schwertmann, U. and Fischer, W. R. (1973) Natural "amorphous" ferric hydroxide. *Geoderma* **10**, 237–247.
Schwertmann, U., Schulze, D. G. and Murad, E. (1982) Identification of ferrihydrite in soils by dissolution kinetics, differential X-ray diffraction, and Mössbauer spectroscopy. *Soil Sci. Soc. Am. J.* **46**, 869–875.
Sherman, D. M. and Randall, S. R. (2003) Surface complexation of arsenic(V) to iron(III) (hydr)oxides: structural mechanism from abinitio molecular geometries and EXAFS spectroscopy. *Geochim. Cosmochim. Acta* **67**, 4223–4230.
Stephens, S. R., Alloway, B. J., Carter, J. E. and Parker, A. (2001a) Towards the characterisation of heavy metals in dredged canal sediments and an appreciation of 'availability': two examples from the UK. *Environ. Pollut.* **113**, 395–401.
Stephens, S. R., Alloway, B. J., Parker, A., Carter, J. E. and Hodson, M. E. (2001b) Changes in the leachability of metals from dredged canal sediments during drying and oxidation. *Environ. Pollut.* **114**, 407–413.
Strawn, D., Doner, H., Zavarin, M. and McHugo, S. (2002) Microscale investigation into the geochemistry of arsenic, selenium, and iron in soil developed in pyritic shale materials. *Geoderma* **108**, 237–257.
van der Zee, C., Roberts, D. R., Rancourt, D. G. and Slomp, C. P. (2003) Nanogoethite is the dominant reactive oxyhydroxide phase in lake and marine sediments. *Geology* **31**, 993–996.

van Gerven, T., Van Baelen, D., Dutré, V. and Vandecasteele, C. (2004) Influence of carbonation and carbonation methods on leaching of metals from mortars. *Cement and Concrete Research* **34**, 149–156.

Yin, C. Y., Mahmud, H. B. and Shaaban, M. G. (2006) Stabilization/solidification of lead-contaminated soil using cement and rice husk ash. *Journal of Hazardous Materials* **137**, 1758–1764.

Yu, Q., Nagataki, S., Lin, J., Saeki, T. and Hisada, M. (2005) The leachability of heavy metals in hardened fly ash cement and cement-solidified fly ash. *Cement and Concrete Research* **35**, 1056–1063.

Zheng, G., Takano, B., Kuno, A. and Matsuo, M. (2001) Iron speciation in modern sediment from Erhai Lake, southwestern China-redox conditions in an ancient environment. *Appl. Geochem*. **16**, 1201–1213.